Optics Letters

Ultra-compact polarization beam splitter utilizing a graphene-based asymmetrical directional coupler

Tian Zhang,[1] Xiang Yin,[1] Lin Chen,[1,*] and Xun Li[2]

[1]Wuhan National Laboratory for Optoelectronics, Huazhong University of Science and Technology, Wuhan 430074, China
[2]Department of Electrical and Computer Engineering, McMaster University, 1280 Main Street West, Hamilton, Ontario L8S, Canada
*Corresponding author: chen.lin@mail.hust.edu.cn

Received 19 October 2015; revised 4 December 2015; accepted 5 December 2015; posted 8 December 2015 (Doc. ID 252252); published 12 January 2016

A novel ultra-compact polarization beam splitter (PBS) utilizing an asymmetrical directional coupler with a combination of a silicon waveguide (SW) and a graphene multilayer embedded silicon waveguide (GMESW) has been proposed and investigated. The modal characteristics of the GMESW for the TM mode varies significantly, whereas that for the TE mode changes slightly with respect to the SW, inducing the launched TM mode to directly pass through the SW with little influence from the GMESW, while the TE mode undergoes a strong coupling and is transferred to the GMESW. A designed PBS with an 8.3 μm-long coupler and 200 nm-wide gap separation offers high extinction ratios (18.2 and 21.2 dB) and low insertion losses (0.16 and 0.36 dB) for the thru and cross ports, respectively. The presented PBS also presents the ability to work with variable splitting ratio power for the TM mode by varying the chemical potential of graphene, implying various applications in signal processing on a chip.

OCIS codes: (130.2790) Guided waves; (130.3120) Integrated optics devices; (230.5440) Polarization-selective devices.

http://dx.doi.org/10.1364/OL.41.000356

Silicon-on-insulator (SOI) plays an important role in integrated photonic devices due to its high-refractive index contrast among various waveguide structures and compatibility with mature CMOS-compatible technologies. However, the strong modal birefringence of SOI waveguides usually makes the control of light polarization extremely challenging. To address this issue, a general solution is to build polarization-independent devices using a polarization diversity system consisting of polarization-handling devices [1]. As a pivotal polarization-handling device, the polarization beam splitter (PBS) has attracted much attention in the past decade [2–6]. Generally, a PBS is designed to efficiently split one input beam with two orthogonal polarization states into two output beams with different polarization states. Many types of SOI waveguide-based PBSs have been reported using various schemes, including adiabatic mode evolution [2], multimode interference [3], and the directional coupler (DC) [4–6]. Adiabatic mode evolution and multimode interference provide approaches to construct a PBS with a high extinction ratio (ER) but at the cost of a large-device footprint, which compromises high-density photonic integration on the SOI platform. By using an asymmetric DC (ADC), a PBS can be built with an ultra-compact size, but it inevitably suffers from a narrow bandwidth and tight fabrication tolerance. An ADC can be realized by utilizing two coupling waveguides of different widths or heights [4], or by employing different types of coupling waveguides, such as a silicon waveguide (SW) combined with a plasmonic waveguide [5] or a silicon nanoslot waveguide [6]. The structural parameters of an ADC should be optimized to satisfy the phase-matching condition for one polarization state, resulting in complete cross coupling. Meanwhile, for the orthogonal polarization state, cross coupling can be effectively avoided due to a significant phase mismatching.

Graphene, a monolayer of carbon atoms arranged in a two-dimensional honeycomb lattice, shows great promise for developing highly efficient optoelectronics devices because of its outstanding electrical and optical properties [7,8], including strong interaction with light, high-speed operation, and tunable optical conductivity [9]. By utilization of the strong electro-absorption and electro-refraction effect induced by graphene, various graphene-based SOI modulators have been intensively proposed and demonstrated to be capable of operating with a broad bandwidth and small-device footprint [9–11]. Quite recently, the authors have proposed a graphene-embedded SW TE-pass polarizer with the performance merits including a high ER, an ultra-low insertion loss (IL), and ultra-compactness [12]. In this Letter, we propose and numerically investigate a novel ultra-compact PBS by utilizing an ADC consisting of an SW (as the launched waveguide) and a graphene multilayer embedded silicon waveguide (GMESW). The modal characteristics for the TM mode vary significantly, whereas that for the TE mode changes slightly for the GMESW near the epsilon-near-zero (ENZ) point [11]. Consequently, the launched TM mode can efficiently pass through the SW with little influence from the

GMESW, as the coupling strength between the two waveguides is very weak due to the significant phase mismatching. Meanwhile, originating from a well-satisfied, phase-matching condition for the TE mode, the launched TE mode experiences a strong coupling and finally outputs from the GMESW.

With the assumption of an $\exp(-i\omega t)$ time dependence, the optical response of graphene is characterized by surface conductivity, σ_g, which is related to the chemical potential, μ_c, by the Kubo formula [7]

$$\sigma_g = i\frac{e^2 k_B T}{\pi\hbar^2(\omega + i\tau^{-1})}\left[\frac{\mu_c}{k_B T} + 2\ln\left(\exp\left(-\frac{\mu_c}{k_B T}\right) + 1\right)\right] + i\frac{e^2}{4\pi\hbar}\ln\left[\frac{2|\mu_c| - \hbar(\omega + i\tau^{-1})}{2|\mu_c| + \hbar(\omega + i\tau^{-1})}\right], \quad (1)$$

where k_B is the Boltzmann constant, $\hbar$ is the reduced Planck's constant, λ is the wavelength (angular frequency ω), T is temperature, e is the electron charge, and τ is momentum relaxation. In our work, $T = 300$ K and $\tau = 0.5$ ps. An electron mobility of $100,000\ \mathrm{cm^2\,V^{-1}\,s^{-1}}$ has been experimentally verified in high-quality suspended graphene [13]. Since this leads to $\tau > 1.5$ ps, the choice of $\tau = 0.5$ ps here is rather conservative. By treating a single sheet of graphene as an ultrathin film [8], its equivalent permittivity (ε_g) can be written as $\varepsilon_g = 1 + i\sigma_g\eta_0/(k_0 d_g)$, which has been extensively employed to characterize the optical property of graphene and estimate the electro-optical properties of graphene-based photoelectric devices both theoretically and experimentally [11,14]. Here $\eta_0(\approx 377\ \Omega)$ is the impedance of air and d_g (0.34 nm) is the thickness of graphene. Around $\mu_c = 0.4$ eV, both the real and imaginary parts of the effective permittivity of graphene [$\mathrm{Re}(\varepsilon_g)$ and $\mathrm{Im}(\varepsilon_g)$] at 1.55 μm vary sharply [12]. More interestingly, the absolute value of ε_g approaches zero at $\mu_{c0} = 0.5$ eV, which is the so-called ENZ point [10]. The graphene monolayer behaves like an ultrathin dielectric material [$\mathrm{Re}(\varepsilon_g) > 0$] below $\mu_c = \mu_{c0}$, while it acts like a metallic layer above $\mu_c = \mu_{c0}$ [$\mathrm{Re}(\varepsilon_g) < 0$].

It has been extensively demonstrated that a graphene/dielectric multilayer can be designed to be highly anisotropic, i.e., the permittivities along the parallel and vertical directions are quite different [15]. This suggests that the propagation characteristics of different polarizations can be very distinctive when a graphene multilayer is involved in an optical waveguide [10]. The present alternating graphene/silicon multilayer [shown in the inset of Fig. 1(a)] is assumed to be infinite in the parallel direction. As a result, it can be treated as a uniform anisotropic material with the permittivity tensor given by $\varepsilon_{\parallel} = (h_g\varepsilon_g + h_d\varepsilon_d)/(h_g + h_d)$ and $\varepsilon_{\perp} = (h_g + h_d)\varepsilon_g\varepsilon_d/(h_d\varepsilon_g + h_g\varepsilon_d)$, where $\varepsilon_{\parallel}$ and $\varepsilon_{\perp}$ denote the permittivities along the parallel and vertical directions, respectively, and ε_d is the permittivity of silicon. Here undoped amorphous silicon is chosen, and its relative permittivity is about 12.04.

Considering the challenge of growing the low-doping concentration of silicon layer with current deposition technology, we can simply deposit an ultrathin insulator (e.g., Al_2O_3) between graphene and silicon to avoid the effect of the silicon layer on graphene's electro-optical properties [16]. Around $\mu_c = 0.4$ eV, as both values of $\varepsilon_{\parallel}$ [Fig. 1(a)] and $\varepsilon_{\perp}$ [Fig. 1(b)] show obvious changes due to the significant variation of ε_g [10]. By contrast, $\varepsilon_{\perp}$ undergoes a very rapid increase around the ENZ point as the electric field polarizes along the vertical

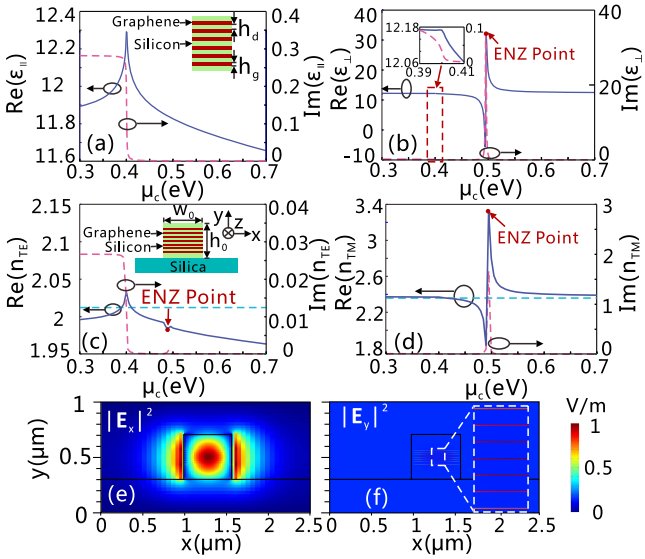

Fig. 1. (a), (b) The parallel (a) and vertical (b) permittivities of an alternating graphene/silicon multilayer vary with μ_c at $\lambda = 1.55$ μm. The inset in (a) is the schematic of an alternating graphene/silicon multilayer, where the thickness of silicon, h_d, is 20 nm. The inset in (b) represents the amplified region of $\varepsilon_{\perp}$ with μ_c varying from 0.39 eV to 0.41 eV. (c), (d) The calculated effective indices of the TE (c) and TM (d) modes in GMESW as a function of μ_c by an eigenmode solver with a commercial software Lumerical MODE Solutions, where $w_0 = 300$ nm and $h_0 = 402.4$ nm. The inset in (c) is the schematic of a GMESW on a silica substrate ($n = 1.48$). (e), (f) The electric field intensity distributions of $|\mathbf{E}_x|^2$ for the TE mode (e) and $|\mathbf{E}_y|^2$ for the TM mode (f).

direction, while $\varepsilon_{\parallel}$ suffers a rather gentle variation. When such a multilayer is inserted into an SW to form a GMESW [see the inset of Fig. 1(c)], it is supposed to have a much larger influence on the modal characteristics of the TM mode than on that of the TE mode. Figures 1(c) and 1(d) show the dependence of the modal characteristics of the GMESW on μ_c. It can be seen that the effective mode index of the TM mode is enhanced to 3.33 at the ENZ point, producing a difference of 0.93 with the SW (without graphene). Meanwhile, the effective mode index of the TE mode undergoes a very tiny variation (0.025). The fact that the graphene layer has a quite different influence on different polarizations of the SW at $\mu_c = 0.5$ eV can be easily understood from the modal field distributions [Figs. 1(e) and 1(f)]. For the TM mode, the electric field (dominated by $\mathbf{E}_y$) will be squeezed into the graphene layers according to Maxwell's boundary conditions [see Fig. 1(f)], hence effectively increasing the effective mode index due to the enhanced graphene-light interaction [10,11]. As for the TE mode, the embedded graphene multilayer almost does not affect the electric field distribution (dominated by $\mathbf{E}_x$) [see Fig. 1(e)] with respect to the SW without graphene, leading to a slight variation of the modal characteristics.

Bearing these points in mind, we propose to construct a PBS by utilization of an ADC consisting of an SW and a GMESW [Fig. 2]. For this ADC, it leads to a larger variation in the modal characteristics for both of the TM and TE modes if more graphene layers are used [12]. The modal characteristics increase with the gap distance between the adjacent graphene layers, h_d,

and reaches the maximum at $h_d = 50$ nm for the TE mode and $h_d = 30$ nm for the TM mode [Figs. 3(a)–3(d)]. Then the influence of the modal characteristics will be weakened as h_d is further enhanced because the graphene layers on the top and bottom tend to have less interaction with the modal field. To produce significant phase mismatching for the TM mode and low-absorption loss for the TE mode simultaneously, a seven-pair graphene/silicon multilayer with $h_d = 20$ nm is chosen. The first, third, fifth, and seventh graphene layers are extended to contact one metal electrode [see the inset (1) of Fig. 2], and the remaining layers contact the other one [see the inset (2) of Fig. 2]. It is worth noting that, the electrostatically induced charge accumulation on graphene's edges due to the utilization of finite width can be effectively avoided by extending the graphene width to connect the metal electrodes [17]. For the fabrication of the PBS, we can first prepare three shadow masks for the SW and two metal electrodes. By properly arranging the order of the three masks, choosing the deposition methods and transferring the graphene layers (etched to "L" shape by a focused ion beam without the utilization of masks) from the copper foil, the presented PBS might be fabricated.

The gate voltage applied on graphene can be obtained through $|\mu_c| = \hbar v_F \sqrt{\pi \varepsilon_d \varepsilon_0 |V_g - V_{\mathrm{Dirac}}|/(h_d e)}$ [11], where the Fermi velocity $v_F \approx 1 \times 10^6$ m/s, and $|V_g - V_{\mathrm{Dirac}}|$ would be the applied voltage because V_{Dirac} is closed to zero. As shown in Fig. 3(e), $\mu_c = 0.5$ eV could be achieved with a bias voltage of 4.6 V, which is comparable to that in graphene-based SOI modulators [10,11,16]. We have noted in the experimental study on SW modulators based on two-layer graphene [16], a chemical potential of about 0.5 eV could be obtained with a bias voltage of 6.5 V, corresponding to the electrical intensity of about 1.3 GV/m. As for our case, the largest electrical field intensity is only 0.58 GV/m with the maximum bias voltage of 11.7 V (associated with the largest chemical potential of 0.8 eV), implying the feasibility of implementing the PBS in practice. After numerical optimization, the width of SW is chosen as 297 nm to ensure that the phase-matching condition is well satisfied for the TE mode [Fig. 3(f)]. Thus a large ERfor the TM mode can be highly expected. With the proper design of the coupler length, the transferred TE mode will output from the cross port with a maximum power. Meanwhile, the TM mode undergoes little influence when passing through the coupling region due to significant phase mismatching and hence outputs efficiently from the thru port. An SW is connected at the end of the GMESW to output the TE mode.

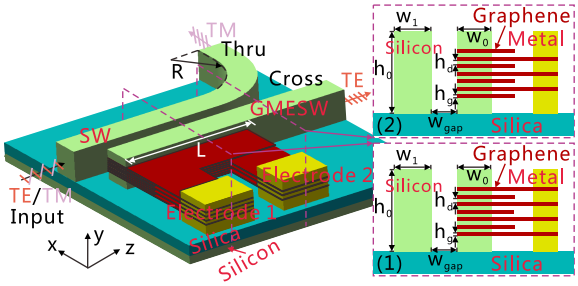

Fig. 2. Schematic configuration of the proposed PBS. The insets (1) and (2) are the cross sections for the coupling region where odd (1) and even (2) numbers of graphene layers attached to metal electrodes.

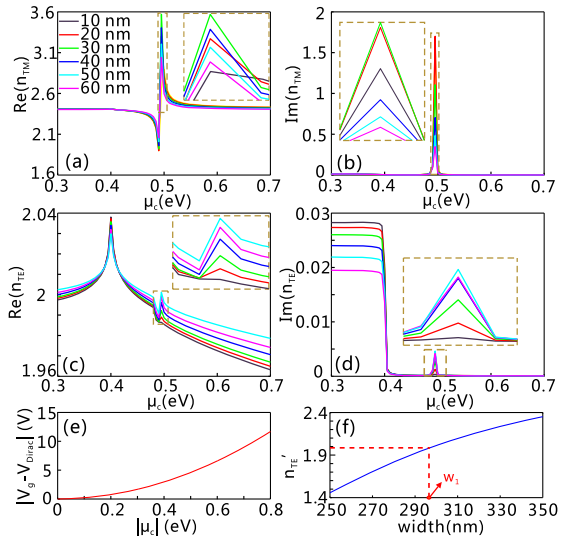

Fig. 3. (a)–(d) The real and imaginary parts of the effective refractive index of the TE (a), (b) and TM (c), (d) modes of GMESW as a function of chemical potential at wavelength of 1.55 μm with different h_d. The insets in (a)–(d) are the amplified region bounded by the yellow-green dashed line rectangles. The layer number of graphene is seven. Here we fix the middle layer of graphene at the center of GMESW. (e) Applied voltage versus μ_c. (f) Effective mode indices of the TE mode, n'_{TE}, as a function of the width of SW. When $w_1 = 297$ nm, the n'_{TE} is equal to the $R(n_{\mathrm{TE}})$ of GMESW with $w_0 = 300$ nm.

At the end of the straight SW, a 90° bent section is connected to make the two output waveguides decoupled. The bending radius, R, is numerically optimized to ensure the TM and TE modes efficiently output through the thru port and through the cross port, respectively. In our work, a bending radius of 1.3 μm has been used to design the PBS, which induces the transmission of the TM mode at the thru port and that of the TE mode at the cross port at 97% and 99%, respectively.

It can be seen from Fig. 4(a) that, with the varied gap separation, the effective mode index of the even/odd TM mode is almost equal to that of individual GMESW/SW, which implies that the TM mode undergoes very weak coupling. On the contrary, the even/odd TE mode has a considerable discrepancy with the TE mode of individual GMESW/SW, indicating strong coupling occurs for the TE mode. To get the maximum-power transfer of the TE mode from the SW to the GMESW, the length of the coupling region should be chosen around the coupling length $L_c = \pi/[k_0(n_{\mathrm{even}} - n_{\mathrm{odd}})]$, where n_{even} (n_{odd}) and k_0 are the effective mode index of even (odd) supermode for the TE mode and the wave number in air, respectively. It can be seen that the difference between the effective mode indices of the two TE supermodes significantly reduces as w_{gap} increases [Fig. 4(a)], corresponding to an exponentially increasing L_c [Fig. 4(b)]. For the design of the PBS with a compact size and relatively good fabrication tolerance, a modest gap separation, w_{gap}, should be chosen. Here w_{gap} is chosen as 200 nm, corresponding to the coupling length of 9.4 μm. Numerical simulation results demonstrate the maximum transmission efficiency (–0.16 dB) for the TE mode occurs at 8.3 μm, and the transmission for the TM mode is not sensitive to the length of the coupling region [Fig. 4(c)]. Therefore, we have designed the directional coupler with the length of 8.3 μm. In our finite

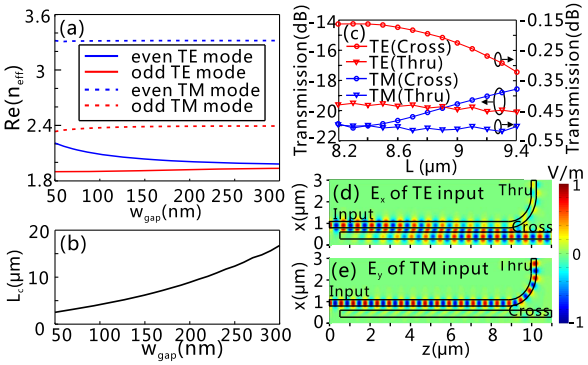

Fig. 4. (a) Effective mode indices of the even and odd TE modes (solid lines) and TM modes (dashed lines) as a function of w_{gap}. (b) Coupling length (L_c) of the TE mode versus w_{gap}. (c) Transmission versus the length of coupling region (L) for the TE and TM modes at two output ports, respectively, with $w_1 = 297$ nm, $w_0 = 300$ nm, $w_{gap} = 200$ nm and $\mu_c = 0.5$ eV. (d), (e) Light propagation in the designed PBS for two polarizations at $L = 8.3$ μm: (d) $\mathbf{E}_x$ distribution of the TE mode and (e) $\mathbf{E}_y$ distribution of the TM mode. The wavelength is 1.55 μm. The simulation of light propagation characteristics (c)–(e) is conducted by FDTD with a commercial software Lumerical FDTD Solutions.

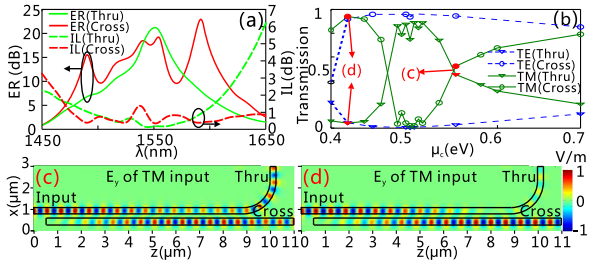

Fig. 5. (a) Wavelength dependence of the designed PBS at $\mu_c = 0.5$ eV. (b) Transmission versus μ_c for the TE and TM modes at two output ports, respectively. $\mathbf{E}_y$ distribution of the TM mode with $\mu_c = 0.55$ eV (c) and $\mu_c = 0.42$ eV (d).

difference time domain (FDTD) simulation, four mesh grids are used to denote the thickness of each graphene sheet. Figure 4(d) clearly indicates the launched TE mode experiences a strong coupling in the coupling section and finally outputs from the cross port. As for the launched TM mode shown in Fig. 4(e), it efficiently passes through the SW with little influence from the GMESW and finally outputs from the thru port. We can achieve ERs of 18.2 and 21.2 dB, and ILs of 0.16 and 0.36 dB for the cross and thru ports, respectively. Here the ERs and ILs are defined as the same as that in [18].

Figure 5(a) shows the wavelength dependence of the ERs and ILs for the designed PBS at the cross and thru ports. One can see that the TM mode is more wavelength-sensitive as shown by the IL at the thru port because of the large wavelength-sensitive mode characteristics for the TM mode in GMSEW, leading to a wavelength-sensitive ER at the cross port. The present PBS has a high ER (>9.5 dB) and low IL (<2.3 dB) for the cross port over broadband wavelength ranges (1481–1616 nm), and a high ER (>9.5 dB) and low IL (<1.4 dB) for the thru port within the range of 1511–1585 nm. These values are superior to or comparable to those previously proposed PBS on the SOI platform [5,18]. More interestingly, the designed PBS also presents the capability of working with variable splitting ratio power for the TM mode by tuning the μ_c of graphene, while the splitting ratio power for the TE mode almost stays still above 0.42 eV [Fig. 5(b)]. Especially, it can function as a 3 dB coupler [$\mu_c = 0.55$ eV, Fig. 5(c)] or a directional coupler [$\mu_c = 0.42$ eV, Fig. 5(d)] for the TM mode, implying various potential applications in signal processing on the SOI platform.

In conclusion, a novel ultra-compact PBS has been proposed and demonstrated by utilization of an ADC consisting of an SW and GMESW. For the present design, the coupler length is chosen to be 8.3 μm when the gap separation is 200 nm. The presented PBS has high ERs (18.2 and 21.2 dB) and low ILs (0.16 and 0.36 dB) for the thru and cross ports at 1.55 μm, respectively. It should be noted that graphene offers the extra dimension of chemical potential tunability, which enables the designed PBS to operate with variable splitting ratio power for the TM mode without reoptimizing and refabricating the device structures. Additionally, under the chemical potential tuning of graphene, it can be highly expected that the PBS undergoes less wavelength dependence and larger fabrication tolerance as opposed to previous PBSs [2–4].

Funding. National Natural Science Foundation of China (NSFC) (11104093, 11474116); The Fundamental Research Funds for the Central Universities (HUST: 2015TS074); Director Fund of WNLO.

REFERENCES

1. H. Fukuda, K. Yamada, T. Tsuchizawa, T. Watanabe, H. Shinojima, and S. Itabashi, Opt. Express **16**, 4872 (2008).
2. M. R. Watts, H. A. Haus, and E. P. Ippen, Opt. Lett. **30**, 967 (2005).
3. H. Jung Moo, R. Hyun Ho, P. Soon Ryong, J. Jae Wan, S. G. Lee, L. El-Hang, P. Se-Geun, W. Deokha, K. Sunho, and O. Beom-Hoan, IEEE Photon. Technol. Lett. **15**, 72 (2003).
4. L. Gao, F. Hu, X. Wang, L. Tang, and Z. Zhou, Appl. Phys. B **113**, 199 (2013).
5. X. Guan, H. Wu, Y. Shi, L. Wosinski, and D. Dai, Opt. Lett. **38**, 3005 (2013).
6. S. Lin, J. Hu, and K. B. Crozier, Appl. Phys. Lett. **98**, 151101 (2011).
7. P. Y. Chen and A. Alù, ACS Nano **5**, 5855 (2011).
8. A. Vakil and N. Engheta, Science **332**, 1291 (2011).
9. K. Kim, J. Y. Choi, T. Kim, S. H. Cho, and H. J. Chung, Nature **479**, 338 (2011).
10. R. Hao, W. Du, H. Chen, X. Jin, L. Yang, and E. Li, Appl. Phys. Lett. **103**, 061116 (2013).
11. S. Ye, Z. Wang, L. Tang, Y. Zhang, R. Lu, and Y. Liu, Opt. Express **22**, 26173 (2014).
12. X. Yin, T. Zhang, L. Chen, and X. Li, Opt. Lett. **40**, 1733 (2015).
13. K. I. Bolotin, K. J. Sikes, Z. Jiang, M. Klima, G. Fudenberg, J. Hone, P. Kim, and H. L. Stormer, Solid State Commun. **146**, 351 (2008).
14. S. Cakmakyapan, H. Caglayan, and E. Ozbay, Carbon **80**, 351 (2014).
15. K. Sreekanth, A. De Luca, and G. Strangi, Appl. Phys. Lett. **103**, 023107 (2013).
16. M. Liu, X. Yin, and X. Zhang, Nano Lett. **12**, 1482 (2012).
17. F. Vasko and I. Zozoulenko, Appl. Phys. Lett. **97**, 092115 (2010).
18. J. Chee, S. Zhu, and G. Lo, Opt. Express **20**, 25345 (2012).